coatings

MDPI

Article

Effect of the Surface States of 1Cr18Ni9Ti Stainless Steel on Mn-Based Brazing Alloy Wetting

Chenghao Zhang [1], Huize Chen [2], Weipeng Yang [2], Qinlian Zhang [2], Bo Yang [2], Yazhen Hu [2], Chun Li [1,*], Dejun Gao [1], Xiaoqing Si [1], Junlei Qi [1] and Jian Cao [1]

[1] State Key Laboratory of Advanced Welding and Joining, Harbin Institute of Technology, Harbin 150001, China
[2] Xi'an Space Engine Company Limited, Xi'an 710021, China
* Correspondence: chun.li@hit.edu.cn

Abstract: The wetting properties of the brazing filler on the substrates play an important role in achieving a reliable joint. In this work, the wetting behaviour of the Mn-based brazing alloy on the surface of 1Cr18Ni9Ti stainless steel is investigated. First, surface treatment was adopted to prepare four different surface states on the stainless steel, including polished, acid treatment, nickel coating, and sandblasting. The surface morphology with nickel coating shows micro-and nano-scale protrusions, forming a uniform 3D Ni layer. The surface roughness of substrates increases after sandblasting treatment. It is found that the wetting angle of brazing alloy on the Ni coated substrates decreases noticeably. After sandblasting, the high roughness speeds up the wetting spread of the brazing alloy at the initial stage. The effect of heating temperature and holding time is also studied systematically. With the increase in holding time, the height of the melting brazing alloy decreases slightly on the sample surfaces. Based on the characterization of the joint section, the Ni layer dissolves into the melting brazing alloy. The diffusion and dissolving are indicated between the brazing alloy and substrates, forming a reliable bond.

Keywords: 1Cr18Ni9Ti; surface state; wetting; Mn-based brazing alloy

Citation: Zhang, C.; Chen, H.; Yang, W.; Zhang, Q.; Yang, B.; Hu, Y.; Li, C.; Gao, D.; Si, X.; Qi, J.; et al. Effect of the Surface States of 1Cr18Ni9Ti Stainless Steel on Mn-Based Brazing Alloy Wetting. *Coatings* **2022**, *12*, 1328. https://doi.org/10.3390/coatings12091328

Academic Editor: Juan Creus

Received: 8 July 2022
Accepted: 26 August 2022
Published: 12 September 2022

1. Introduction

Stainless steel is widely applied in various applications due to its excellent corrosion resistance [1–3]. Welding and joining are always carried out to fabricate complex stainless steel structures [4,5]. Compared with other joining methods, brazing introduces less effect on the base material since the heating temperature is lower than the melting point of substrates [6,7]. The alloy must have good wetting behaviour on the sample surfaces when brazing [8,9]. Therefore, it is essential to carry out systematic research on the wetting behaviour between brazing alloys and base substrates. To improve the wetting properties, surface treatment, such as modification layer and microstructure fabrication on the surfaces of the substrates, has attracted a lot of attention [10–12].

Stainless steel is mainly composed of the elements Fe, Cr, Ni, etc., [13–15]. The suitable alloy for brazing stainless steel includes Ag-based [16], Ni-based [17], Mn-based [18], and Cu-based brazing alloy [19]. Mn-based alloy is commonly used as the brazing alloy for stainless steel because of its good mechanical properties and excellent high-temperature performance [20]. The good wetting ability, oxidation resistance, and high strength joint of Mn-based alloy make it widely used in real industrial applications [21]. Li et al. [22] studied the brazing of copper and stainless steel by using Mn-related filler, achieving an enhanced tensile strength of the joint.

Based on Young's equation, the contact angle of melting brazing alloy on the sample surfaces could be calculated by the interface energy of solid-liquid, liquid-gas, and solid-gas [23]. The modification layer on the substrates, such as Ni [24], Au [25], Cu coatings [26], etc., can improve the wetting properties of the brazing alloy via change of the solid-related

interface energy. Considering the cost and the compatibility between Fe and Ni elements, the Ni coating is always prepared as the modification layer on the stainless steel [27–29]. Furthermore, Ni has good solid solubility with many other elements, such as Ag [30], Mn [31], Cu [32], etc., indicating that the Ni layer could form a strong bond with a variety of brazing alloys. Venkateswaran [33] revealed that Ni coating could obviously decrease the contact angle of brazing alloys on the base metal, further improving the shear strength of the brazing joint.

Wenzel and Cassie's theory provides another strategy to decrease the contact angle of melting brazing alloy [34,35]. If the liquid contact angle on the flat surface is lower than 90°, improving the roughness is beneficial for decreasing the contact angle. Numerous methods, such as chemical etching [36–38], laser manufacturing [39,40], electrodeposition [41,42], and machining [43], have all been investigated as ways to fabricate well-arranged or randomly distributed microstructures on the metal surface. Tan et al. [44] analyzed the effect of chemical-etched textures on the wetting behaviour of melting brazing alloy. The improved surface roughness promotes spreading speed and bond strength. Yu et al. [45] fabricated different surface textures on stainless steel substrates by laser, including micro-grooves, micro-pits, and micro/nano-ripples. During the wetting process, the micro-textures have been proven to increase the contact angle and the reaction layer thickness. It can be seen that the surface treatment has been explored in the field of brazing stainless steel. However, there is limited research on the comprehensive effect of both surface roughness and modification on wettability.

In this paper, 1Cr18Ni9Ti stainless steel with four surface states was first prepared, including acid treated, Ni coated with different thickness, and sandblasted. The phase and surface morphology of substrates were characterized by SEM, XRD, and confocal laser scanning microscopy. The contact angle of the brazing alloy was measured using both in situ and ex situ approaches. The effect of brazing parameters on the wetting behaviour of the Mn-based brazing alloy was studied systematically. The phase and microstructure of the interface between brazing alloy and substrates were analysed carefully by SEM and EDS.

2. Experimental Section

2.1. Wetting Experiment

The chemical composition of 1Cr18Ni9Ti substrates and Mn-based brazing alloy is shown in Table 1. The 1Cr18Ni9Ti plate was cut into small pieces (45 mm × 45 mm × 2 mm) and divided into four groups. The first group of samples were treated with acid. The second group contains acid treatment and 4 μm-Ni coatings. The third and fourth groups are acid treatment + 10 μm-Ni and sandblasting + 4μm-Ni, respectively. As shown in Figure S1, the Mn-based brazing alloy was placed on the sample surface and heated in a chamber with a vacuum better than 5×10^{-3} Pa to test the wetting properties. Both the heating and cooling rates are 15 °C/min. In our preliminary work, the Mn-based brazing alloy could exhibit good flowing and wetting performance when the heating temperature exceeds 1100 °C. When the holding time is too short, the joint is not uniform. The ultra-long holding time can lead to an overreaction between the base substrates and brazing alloys. Thus, the heating temperature is set at 1150 °C, 1170 °C, and 1190 °C, with a holding time of 15 min, 25 min, and 35 min.

Table 1. Chemical composition of the base substrate and brazing alloy (wt.%).

Element	Fe	Ni	Cr	Mn	Si	Ti	C
1Cr18Ni9Ti	Bal.	8~11	17~19	≤2.0	≤1.0	0.8	≤0.12
Mn70NiCr	-	24.0~26.0	4.5~5.5	Bal.	-	-	-

2.2. Characterization

After surface treatment, the phases of the samples were analysed by X-ray diffraction (XRD, D8 Advanced, Bruker, Karlsruhe, Germany). A field-emission scanning electronic microscope (FE-SEM, SU5000, Hitachi, Tokyo, Japan) was used to observe the morphology and microstructure of sample surfaces and interfaces. The roughness of the surface was measured by a laser scanning confocal microscope (OLYMPUS, OLS3000, Tokyo, Japan). The element analysis was carried out by an energy dispersive X-ray spectrometer (EDS). The contact angle of the brazing alloy on the sample was measured by an optical contact angle measurement device (OCA20, Dataphysics, Stuttgart, Germany) at ambient temperature. The contact angle at the high-temperature stage was observed in situ by a CCD camera through a transparent window in the furnace.

3. Result and Discussion

3.1. The Characterization of Substrates

Before surface treatment, the base substrates of 1Cr18Ni9Ti stainless steel were characterized and shown in Figure S2. The AFM images in Figure S2a,b indicate that only some scratches can be observed on the surface due to the sandpaper polishing. Figure S2c displays the EDS results of the base substrates, which mainly contain 20.17% Cr, 69.66% Fe, and 9.34% Ni. The phase was analysed by XRD, as shown in Figure S2d. The Fe-Cr and Fe-Ni peaks agree well with the phase of stainless steel. Figure 1a–c illustrates the morphology of substrates after acid treatment. A large number of grains and small gaps can be observed on the sample surface. Figure 1d–f presents the surface topography of the substrates after acid treatment and deposition of a 4 μm thick Ni layer. It can be seen that a series of micro- and nano-scale protrusions are presented on the sample surface. Figure 1g–i shows the SEM images of the substrates after acid treatment and 10μm Ni layer deposition. The morphology is similar to that in Figure 1d–f. However the size of protrusions increases. Figure 1j–l shows the sample surface after sandblasting and Ni deposition. Two-level hierarchical structures can be observed on the sample surfaces. The first-level structure consists of the micro-pits and micro-bulges resulting from the sandblasting treatment. The second-level structure of small protrusions, which grow on the surface of micro-bulges, can be assigned to the Ni deposition. The EDS results of the samples after Ni deposition only show Ni peaks.

The roughness value of the four samples is measured by a confocal microscope, as shown in Figure 2. Figure 2a–d corresponds to the results of the samples after acid treatment, acid treatment + 4 μm Ni, acid treatment + 10 μm Ni, and sandblasting + 4 μm Ni. The surface roughness Ra values of the four samples are 0.1842, 0.1415, 0.1661, and 8.1604, respectively. It can be seen that Ni deposition has little effect on the surface roughness, while sandblasting can significantly increase the roughness value. Figure S3 presents the AFM images of the samples after acid treatment and acid treatment + 4 μm Ni. The surface profile is below 1 μm, further indicating that Ni deposition introduces less effect on the surface roughness value.

The phase composition of the substrates after acid treatment is shown in Figure 3a. Compared with the XRD result in Figure S2d, the intensity ratio between Fe-Cr and Fe-Ni peaks has changed due to the acid etching. For the sample after acid treatment and 4 μm Ni deposition, there is an obvious Ni peak in the XRD result, as shown in Figure 3b. As the thickness of the Ni layer increases, the intensity ratio of the Ni peak also increases, as shown in Figure 3c. Figure 3d displays the XRD result of the sample after sandblasting and 4 μm Ni deposition, in which Ni peaks are more obvious than the Fe-Cr peaks, because the high surface roughness can influence the intensity of XRD.

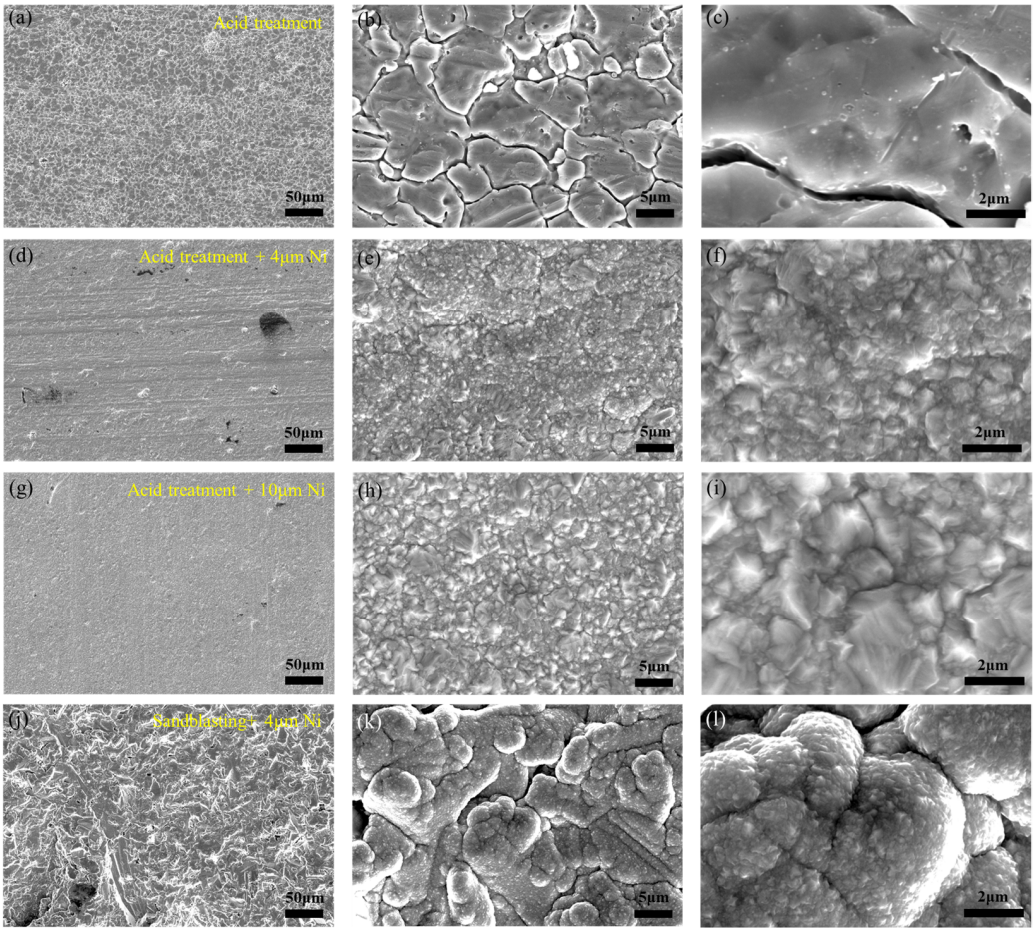

Figure 1. SEM images of 1Cr18Ni9Ti after surface treatment (**a**–**c**) Acid treatment, (**d**–**f**) acid treatment + 4 μm Ni, (**g**–**i**) acid treatment + 10 μm Ni, (**j**–**l**) sandblasting + 4 μm Ni.

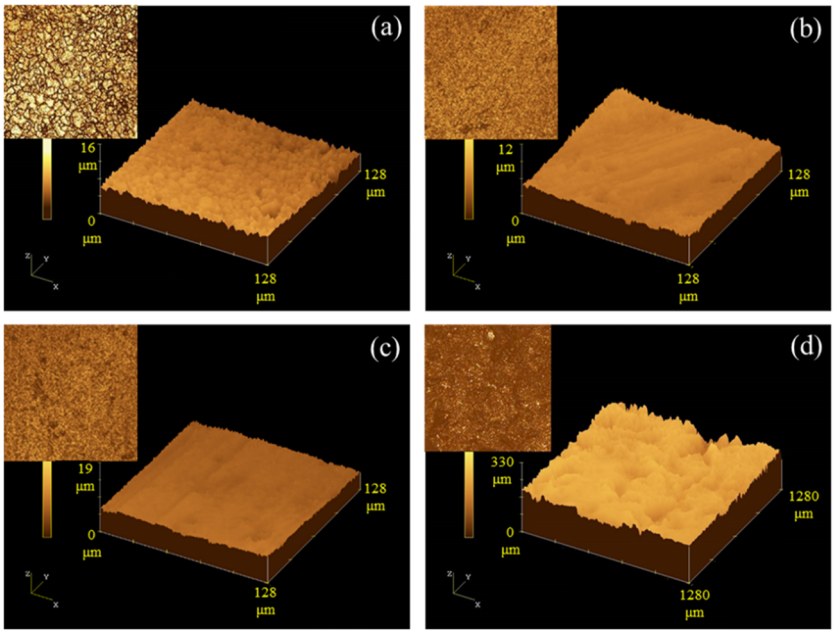

Figure 2. Laser confocal images of stainless steel after surface treatment (**a**) Acid treatment, (**b**) acid treatment + 4 μm Ni, (**c**) acid treatment + 10 μm Ni, (**d**) sandblasting + 4 μm Ni.

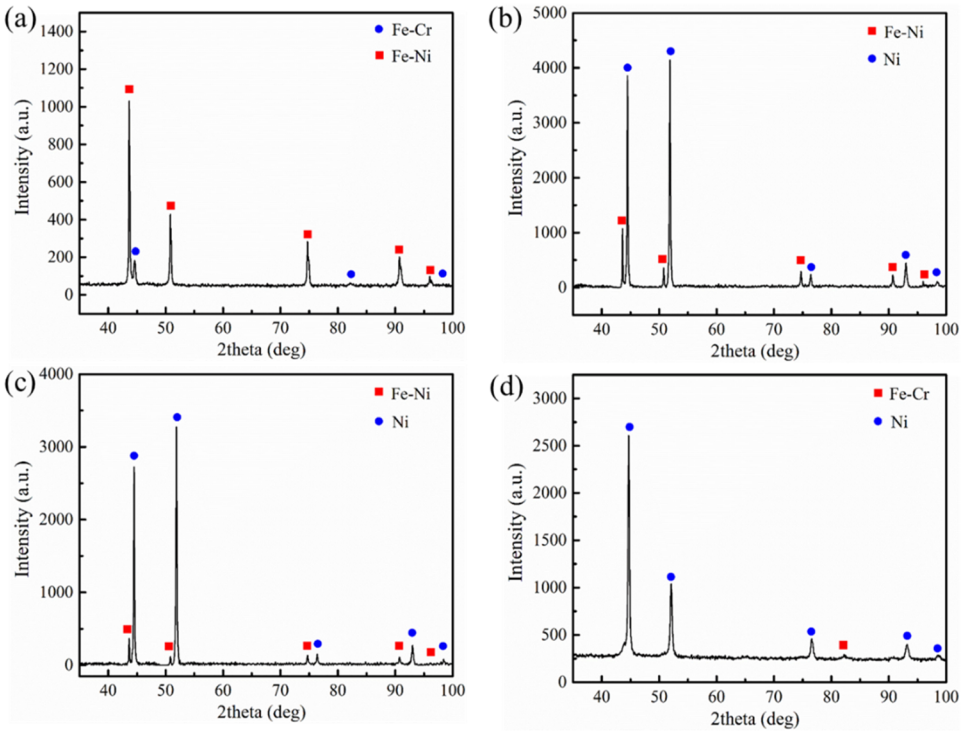

Figure 3. XRD results of stainless steel after surface treatment (**a**) Acid treatment, (**b**) acid treatment + 4 μm Ni, (**c**) acid treatment + 10 μm Ni, (**d**) sandblasting + 4 μm Ni.

3.2. In Situ Observation of the Brazing Alloy Contact Angle

In order to analyse the wetting behaviour and spreading dynamics of the brazing alloy, a real-time wetting angle-measuring device was used to observe the wetting of the brazing alloy. Figure 4 shows the melting and wetting behaviour of the brazing alloy on substrates of acid treatment at 1190 °C/25 min. The shape of the brazing alloy was stable at a temperature of 1060 °C. When it reaches 1070 °C, it can be seen that the brazing alloy has collapsed, and the root is connected with the base substrate, which proves that the brazing alloy begins to melt. Then the brazing alloy agglomerates into a circular arc on the sample surface as the temperature increases. When the temperature reaches 1100 °C, the upper surface becomes completely smooth. It can be regarded as the initial wetting stage. Two minutes are required for the brazing alloy to show a smooth surface on the substrates of the acid treatment since it starts to melt because the heating rate in this experiment is 15 °C/min. The wetting angle of the brazing alloy on the base substrate is 38.1°. Based on the images corresponding to the temperature of 1130 °C, 1150 °C, 1170 °C, and 1190 °C, it can be observed that the contact angle decreases gradually. The contact angle has been reduced to 30.0° at a temperature of 1190 °C. During holding at 1190 °C for 25 min, the results of the brazing alloy wetting angle are measured. Considering the error of fitting calculation, it can be considered that the contact angle of the brazing alloy does not change obviously at this stage. In addition, the height of the brazing alloy at 1100 °C is larger than that at 1190 °C, proving that the brazing alloy and the base metal gradually dissolve and diffuse during the heating process, which is consistent with the change of contact angle. It can be concluded that the dynamic wetting angles of brazing alloy on the substrates decrease rapidly at first and then slowly change, agreeing with previous research [21].

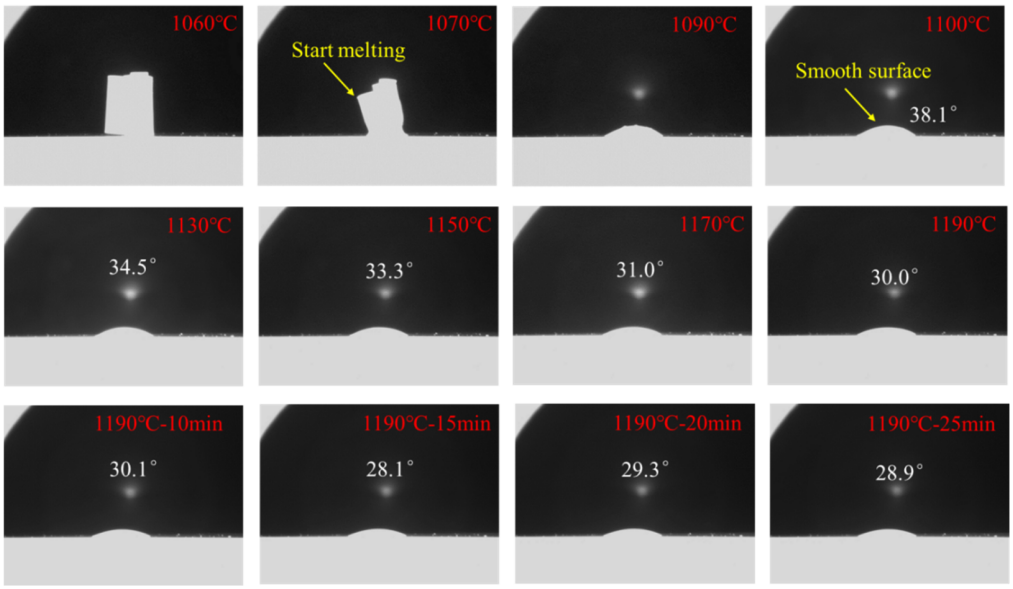

Figure 4. High-temperature contact angle on substrates of acid treatment.

Figure 5 presents the initial stage of brazing alloy wetting on substrates of acid treatment + 4 μm Ni at 1190 °C/25 min. The brazing alloy starts melting at 1070 °C, similar to the sample in Figure 4. However, the brazing alloy could wet and spread fast on the sample surface. When the temperature reaches 1075 °C, a smooth upper surface is obtained. It means that only 1/3 min is used for the brazing alloy to complete the initial wetting stage since it starts to melt on the substrates of acid treatment + 4 μm Ni, indicating that the Ni deposition layer could promote the spreading.

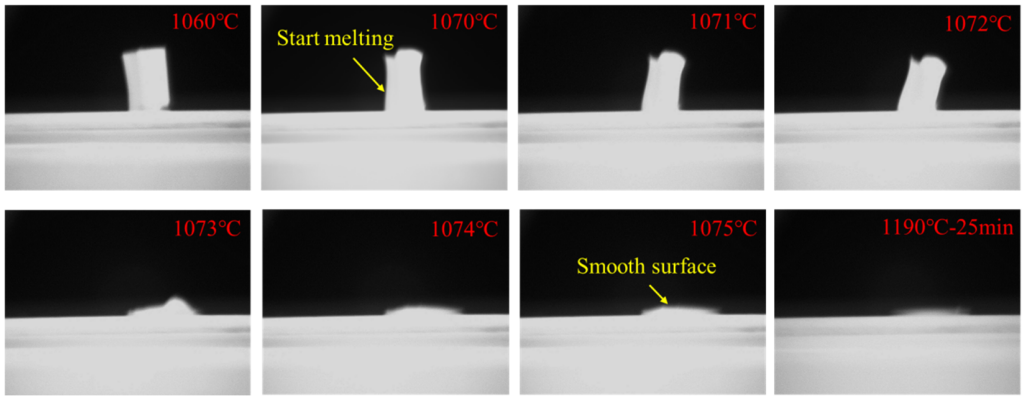

Figure 5. High-temperature contact angle on substrates of acid treatment + 4 μm Ni.

To compare the effect of surface roughness on the wetting behaviour at 1190 °C/25 min, the contact angle of the brazing alloy on substrates of acid treatment + 10 μm Ni and sandblasting + 4 μm Ni were observed at the same time, as shown in Figure 6. After the brazing alloy starts melting at 1070 °C, the brazing alloy completes the initial wetting stage at 1075–1076 °C on the substrates of acid treatment + 10 μm Ni, indicating that the thickness of the Ni layer has a limited effect on the initial wetting stage. Interestingly, the brazing alloy spreads much faster on the substrates of sandblasting + 4 μm Ni. The initial wetting stage is completed at 1072 °C. Since the surface after sandblasting shows the largest surface roughness, it indicates that the high roughness could accelerate the spread process of melting brazing alloy. At 1100 °C, the contact angles of the two samples are 21.8° and 23.4°, respectively. When the temperature increases to 1190 °C, the angles decrease to 16.9° and 18.3°. After holding at 1190 °C for 10 min, the angles decrease to 15.9° and 13.0°. Then the wetting angle generally remains unchanged.

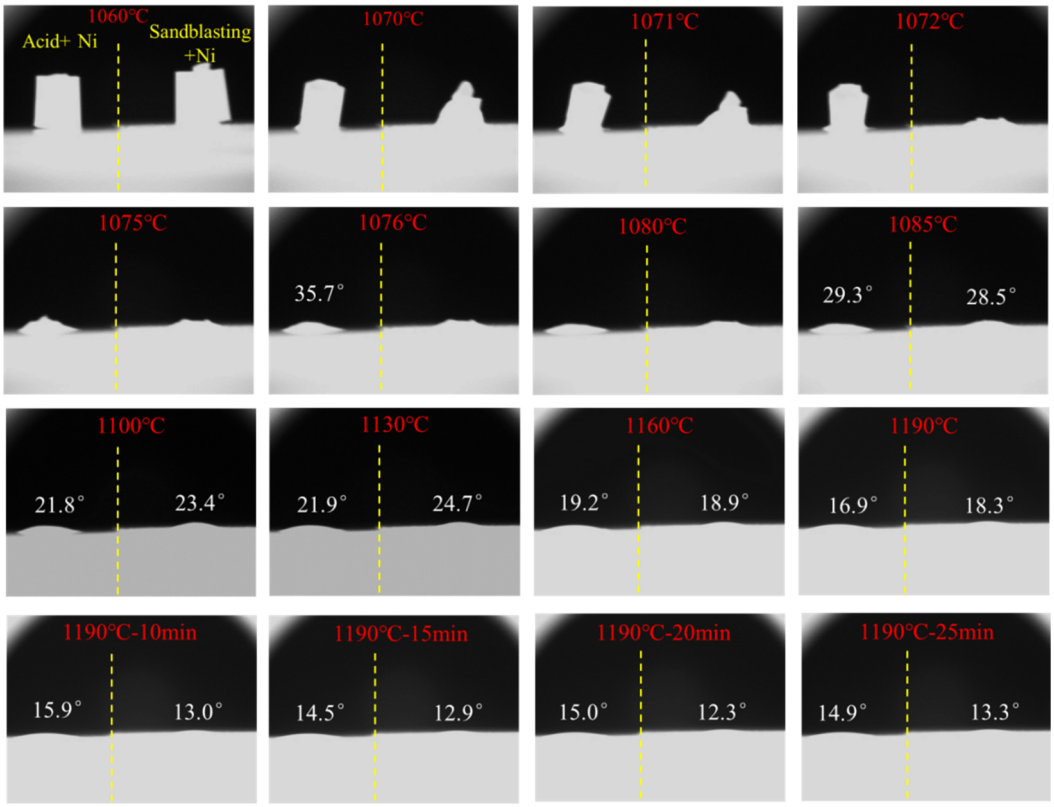

Figure 6. High-temperature contact angle on substrates of acid treatment + 10 μm Ni and sandblasting + 4 μm Ni.

Thus, by analysing the wetting behaviour on different surfaces, it can be seen that the Ni deposition on the stainless steel surface can decrease the contact angle of the brazing alloy. The Ni layer could also accelerate the initial wetting stage. The high roughness further improves the spreading speed of the brazing alloy at the initial wetting stage.

3.3. The Wetting and Spreading Properties

After cooling, the brazing alloy's contact angle and spreading area were measured and listed in Table 2. Since the amount of brazing alloy on each sample is fixed, the contact angle and spreading area are directly related. The better wetting behaviour leads to a smaller contact angle and larger a spreading area.

Firstly, it can be noticed that the samples with Ni layers are more beneficial for the brazing alloy wetting. The contact angles are obviously smaller than those on the samples with only acid treatment, proving the Ni layer can lead to a decrease in contact angles. Based on the results in Section 3.2, the high surface roughness could accelerate the initial wetting stage. However, the final contact angles on the samples with high roughness are roughly similar to those with small roughness. The effect of heating temperature and holding time can also be summarised as follows: (1) When only acid is used to treat the samples, the wetting angles increase slightly and then decrease as the temperature increases; (2) for the samples after acid treatment and Ni deposition, the contact angles decrease as holding time increases; and (3) the effect of heating parameters is not very obvious for the samples after blasting treatment.

Table 2. Contact angle and spreading area of brazing alloy.

1Cr18Ni19Ti No.	Surface States	Contact Angle/Brazing Alloy Spreading Area (mm^2)		
		1150 °C/15 min	1170 °C/15 min	1190 °C/15 min
1	Acid treatment	15.4°/26.463	19.5°/25.092	20.6°/21.264
2	Acid treatment + 4 μm Ni	6.1°/49.662	7.7°/38.031	11.8°/37.532
3	Acid treatment + 10 μm Ni	15.3°/42.318	18°/31.408	14°/28.142
4	Sandblasting + 4 μm Ni	10.4°/36.121	13.3°/30.121	15.3°/26.044
5	Acid treatment	18.9°/26.248	24.7°/18.511	22.4°/23.681
6	Acid treatment + 4 μm Ni	11.6°/39.246	6.4°/45.595	6.6°/41.073
7	Acid treatment + 10μm Ni	7.9°/39.581	12.0°/39.173	11.9°/31.660
8	Sandblasting + 4 μm Ni	13.0°/31.944	11.7°/27.681	8.9°/32.523
9	Acid treatment	20.9°/26.892	24.2°/22.125	20°/23.647
10	Acid treatment + 4 μm Ni	10.1°/38.905	6.3°/51.458	6.6°/43.396
11	Acid treatment + 10 μm Ni	8.2°/40.169	8.6°/45.662	6.3°/57.521
12	Sandblasting + 4 μm Ni	15.1°/32.660	9.1°/39.551	10.1°/32.533

3.4. The Interfacial Microstructure between Brazing Alloy and Substrates

After the wetting experiment, the samples were cut and treated to investigate the cross-sectional interface between brazing alloys and substrates. Figure 7 shows the SEM image and corresponding element map distribution of brazing alloy on substrates of acid treatment at 1170 °C/25 min. The brazing alloy part is composed of Fe, Cr, Mn, and Ni. The base substrate is mainly composed of the elements Fe and Cr. In addition, some Ti-rich points are distributed randomly in the interface. As shown in Figure 7, Table 3 shows the EDS analysis at different points. Point A corresponds to the FeCrNi phase on the top surface of the brazing alloy. Point B contains more Mn compared to point A due to the diffusion of Mn. The chemical composition at point C is similar to that of the base substrate. Point D is basically at the base substrate, which contains 70.10% Fe and 19.56% Cr. A coordinate is built in the Fe element distribution image. The x-axis is the original surface of the substrates. In region IV, the boundary line between the brazing alloy and substrate is below the x-axis, indicating the dissolving of substrates. In region I, the Mn content is lower in the top layer than in the inner part of the brazing alloy. The other element behaved with an opposite distribution trend, showing the diffusion during the wetting process. It is noticeable that the boundaries between brazing alloys and substrates are not easily identified because of the dissolving and diffusion between the molten brazing alloys and solid substrates at the high-temperature stage. The transition area of element change is always at the interface between brazing alloys and substrates in the field of brazing metal [46].

The SEM image and EDS result of brazing alloy on substrates of acid treatment + 4 μm Ni at 1170 °C/25 min are displayed in Figure 8 and Table 4. The microstructures and element distribution are similar to that in Figure 7, except that a Ni layer can be seen in the top layer of substrates, as shown in point C of Figure 8. There is element diffusion between the initial Ni deposition layer and the substrate, resulting in a chemical composition of 49.19% Fe and 40.91% Ni. Points A and B correspond to the different regions of the brazing alloy. Point D is located at the base of the substrates. At the interface between the brazing alloy and the base substrate, the Ni deposition layer on the base substrate is totally dissolved by the brazing alloy.

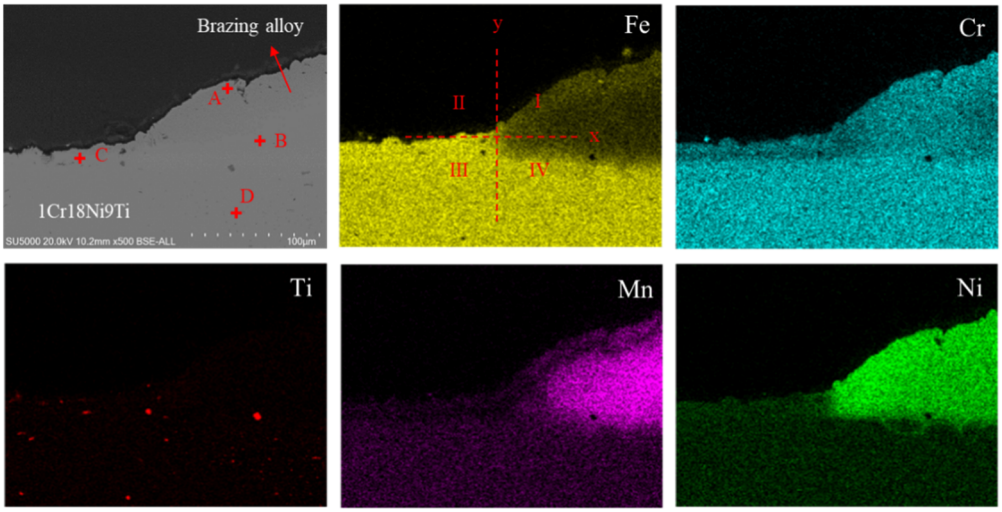

Figure 7. SEM image and the corresponding element map distribution of brazing alloy on substrates of acid treatment at 1170 °C/25 min.

Table 3. The EDS results in Figure 7.

Element (At.%)	Ti	Cr	Mn	Fe	Ni
A	-	17.05	2.59	24.19	56.17
B	-	15.95	24.66	13.88	45.52
C	0.59	12.60	0.39	76.28	10.14
D	0.57	19.56	1.9	70.10	7.95

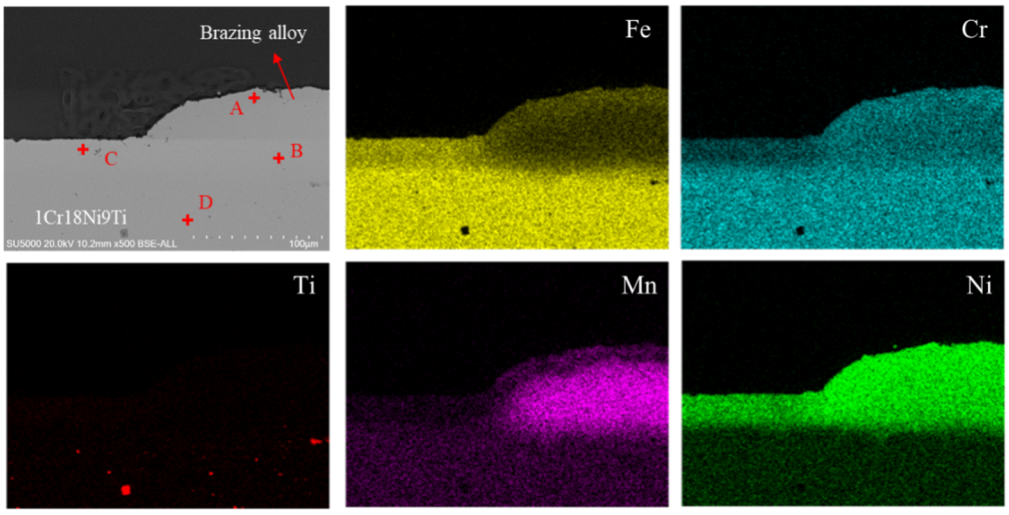

Figure 8. The SEM image and the corresponding element map distribution of brazing alloy on substrates of acid treatment + 4 μm Ni at 1170 °C/25 min.

Table 4. The EDS results in Figure 8.

Element (At.%)	Ti	Cr	Mn	Fe	Ni
A	-	16.06	5.50	21.92	56.53
B	-	14.44	22.37	15.87	47.32
C	1.38	8.21	0.33	49.16	40.91
D	0.65	19.07	1.73	70.69	7.87

The SEM image and EDS results of brazing alloy on substrates of acid treatment + 10 μm Ni at 1170 °C/25 min are shown in Figure 9 and Table 5. It can be seen that the Ni thickness on the substrates has little influence on the wetting behaviour. Point C contains more Ni compared with the same region in Figure 8, because there is a thicker initial Ni deposition layer. The other areas are all similar to those in Figure 8.

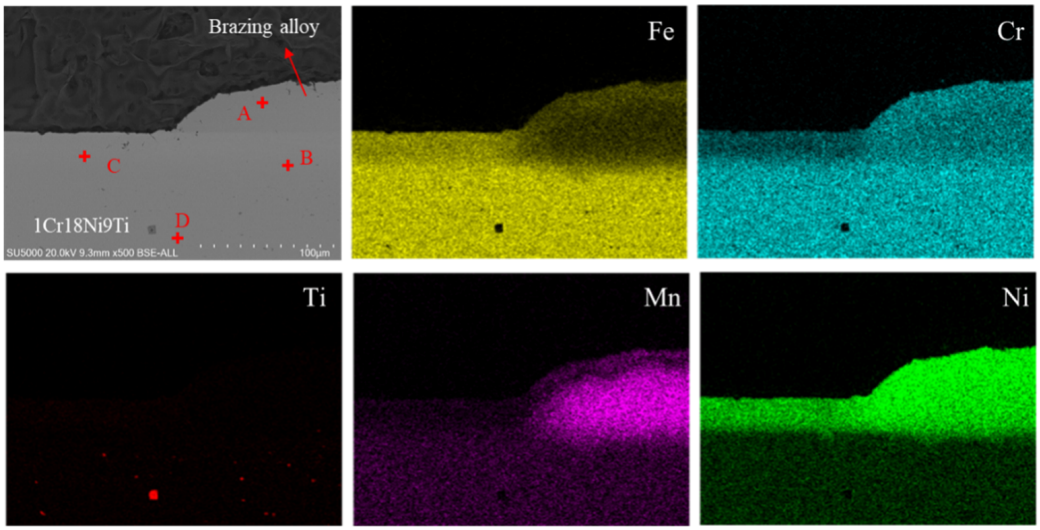

Figure 9. The SEM image and the corresponding element map distribution of brazing alloy on substrates of acid treatment + 10 μm Ni at 1170 °C/25 min.

Table 5. The EDS results in Figure 9.

Element (At.%)	Ti	Cr	Mn	Fe	Ni
A	-	18.38	3.09	22.04	56.49
B	-	13.77	25.23	12.69	48.32
C	1.13	7.73	0	42.4	48.90
D	0.45	19.01	1.67	70.75	8.12

Figure 10 and Table 6 present the SEM image and the corresponding EDS results of brazing alloy on substrates of sandblasting + 4 μm Ni at 1170 °C/25 min. A thin layer is distributed on the surface of the substrates. Point A is mainly composed of the FeCrNi phase. Point B contains the Mn-rich phase based on the FeCrNi phase. (Mn, Ni) solution is a typical phase in the joint of an Mn-based brazing alloy [47]. Point C is approximately at the interface between the brazing alloy and the base of the substrates. The chemical composition at Point D is similar to that in Figures 7–9. A big gap can be observed in the cross-sectional interface, resulting from the sandblasting treatment of the substrates. The border of brazing alloys ends at the edge of the gap. It can be speculated that the melting brazing alloy spreads to the edge of the gaps, and then the flow is prevented by the gap. Therefore, the brazing alloy contact angle on the sample after sandblasting + Ni deposition treatment is smaller than that with only the Ni layer.

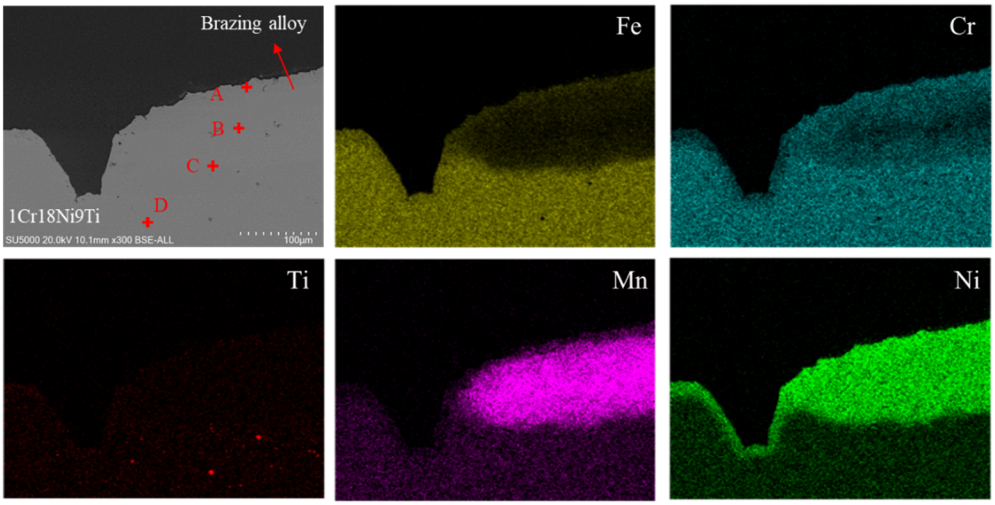

Figure 10. The SEM image and the corresponding element map distribution of brazing alloy on substrates of sandblasting + 4 μm Ni at 1170 °C/25 min.

Table 6. The EDS results in Figure 10.

Element (At.%)	Ti	Cr	Mn	Fe	Ni
A	-	19.06	7.66	21.04	52.25
B	-	10.07	34.57	7.83	47.53
C	6.51	19.52	8.35	52.77	12.84
D	0.65	19.18	1.76	70.20	8.21

Based on the above results, there are several main phenomena observed. The first is that the Ni layer could decrease the contact angle of the brazing alloy on the stainless steel samples. The second is that high surface roughness could further accelerate the initial wetting speed. If the dissolving and diffusion between brazing alloys and substrates are ignored, the effect of surface states on wetting properties can be discussed as follows. The contact angle of the melting brazing alloy on stainless steel substrates at equilibrium can be analysed by Equation (1).

$$\gamma_{lg} \cos\theta = \gamma_{sg} - \gamma_{sl} \quad (1)$$

where γ_{lg}, γ_{sg}, and γ_{sl} are the tension forces of liquid-gas, solid-gas, and solid-liquid, respectively. θ is the contact angle of the brazing alloy on the substrates. When the Ni layer is deposited on the surface of stainless steel substrates, the interface energy and tension force between the substrate and melting brazing alloy have been changed, leading to a decrease in contact angle [33].

The contribution of the surface roughness to the spread of brazing alloy could be explained by Equation (2) proposed by Miao et al. [48].

$$L_0 = \sqrt{\frac{4\pi w \gamma_{lg}\left(\cos\theta - \sin\frac{\beta}{2}\right)}{\lambda(\beta)\eta}} \times \sqrt{t} \quad (2)$$

where η is the viscosity of the melting brazing alloy, and t is the spreading time. Assuming that the shape of microstructures on the surface is a triangle, the side length is w and its open angle is β. The length of the triangle is L. $\lambda(\beta)$ is a geometric parameter corresponding to the angle β.

To simplify the calculation and analysis, the open angle β approximately remains unchanged for the surface with higher roughness. The larger side length of the triangle is w_m. Then the spreading length could be written as Equation (3).

$$L_m = \sqrt{\frac{4\pi w_m \gamma_{lg}\left(\cos\theta - \sin\frac{\beta}{2}\right)}{\lambda(\beta)\eta}} \times \sqrt{t} \tag{3}$$

In this case, the ratio of liquid spreading length on the rough surface and on the relatively flat surface can be concluded.

$$\frac{L_m}{L} = \sqrt{\frac{w_m}{w}} \tag{4}$$

Based on Equation (4), the relationship between L_m/L and w_m/w is shown in Figure 11. The spreading speed of brazing alloys could be improved as w_m increases, indicating the effect of high surface roughness on the spreading of brazing alloys.

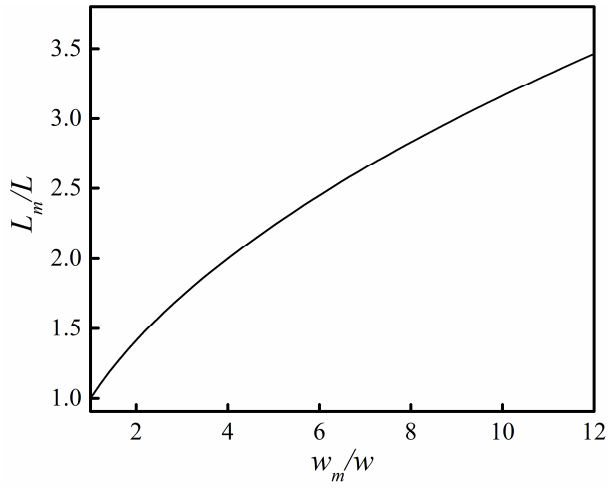

Figure 11. The corresponding calculated ratio of L_m/L as a function of w_m/w.

4. Conclusions

In summary, the wetting behaviour of Mn-based brazing alloy on different surface states of stainless steel has been studied in detail. Acid treatment, Ni deposition, and sandblasting were used to prepare stainless steel with different surface states. After acid treatment, the surface shows a roughness of Ra 0.1842. The Ni deposition introduces a large number of small protrusions, but the roughness value only changes a little. The substrates after sandblasting show a high roughness Ra of 8.1604. When the heating temperature reaches the melting point, the brazing alloy spreads on the sample surface. The Ni deposition could accelerate the initial spread of melting brazing alloy and decrease the final contact angle because the Ni layer could change the interface energy between the brazing alloy and substrates. The initial spreading speed can be further developed by the high roughness after sandblasting. Meanwhile, the Ni layer on the sample surface will be dissolved by melting brazing alloy. Diffusion and dissolving take place between the brazing alloy and substrates. This paper systematically discussed the influence of surface states on the wetting behaviour of brazing alloys, providing a theoretical reference and data support for brazing stainless steel in actual application. Additionally, it is the first time to analyse the mechanism of the surface roughness on the spreading rate of a brazing alloy.

Supplementary Materials: The following supporting information can be downloaded at: https://www.mdpi.com/article/10.3390/coatings12091328/s1, Figure S1: Side view of the base substrate and brazing alloy; Figure S2: Characterization of 1Cr18Ni9Ti base substrates without surface treatment. (a) Two-dimensional AFM image, (b) Three-dimensional AFM image, (c) EDS results, and (d) XRD spectra; Figure S3: AFM images of 1Cr18Ni9Ti base substrates after surface treatment. (a,c) Acid treatment and (b,d) acid treatment + 4 μm Ni.

Author Contributions: Conceptualization, C.L. and H.C.; methodology, H.C. and W.Y.; software, C.Z. and Q.Z.; validation, B.Y., X.S. and J.Q.; formal analysis, C.Z. and C.L.; investigation, Y.H. and D.G.; writing—original draft preparation, C.Z.; writing—review and editing, C.Z. and C.L.; visualization, D.G. and X.S.; supervision, C.L. and J.C.; project administration, J.Q. and C.L.; funding acquisition, J.C. and H.C. All authors have read and agreed to the published version of the manuscript.

Funding: This research was funded by the National Natural Science Foundation of China under Grant No. 52125502, the Fundamental Research Funds for the Central Universities (FRFCU5710051121 and FRFCU5720100421), and the Postdoc Foundation of Heilongjiang Province (LBH-Z18064).

Institutional Review Board Statement: Not applicable.

Informed Consent Statement: Not applicable.

Data Availability Statement: The data presented in this study are available on request from the corresponding author.

Conflicts of Interest: The authors declare no conflict of interest.

References

1. Lodhi, M.; Deen, K.M.; Wacker, M.G.; Haider, W. Additively manufactured 316L stainless steel with improved corrosion resistance and biological response for biomedical applications. *Addit. Manuf.* **2019**, *27*, 8–19. [CrossRef]
2. Dinu, M.; Parau, A.C.; Viadescu, A.; Kiss, A.E.; Pana, I.; Mouele, E.S.M.; Petrik, L.F.; Braic, V. Corrosion Improvement of 304L Stainless Steel by ZrSiN and ZrSi(*N*,*O*) Mono- and Double-Layers Prepared by Reactive Cathodic Arc Evaporation. *Coatings* **2021**, *11*, 1257. [CrossRef]
3. Kong, D.; Dong, C.; Ni, X.; Zhang, L.; Yao, J.; Man, C.; Cheng, X.; Xiao, K.; Li, X. Mechanical properties and corrosion behavior of selective laser melted 316L stainless steel after different heat treatment processes. *J. Mater. Sci. Technol.* **2019**, *35*, 1499–1507. [CrossRef]
4. Zhu, W.; Zhang, H.; Guo, C.; Liu, Y.; Ran, X. Wetting and brazing characteristic of high nitrogen austenitic stainless steel and 316L austenitic stainless steel by Ag–Cu filler. *Vacuum* **2019**, *166*, 97–106. [CrossRef]
5. Khan, M.; Dewan, M.W.; Sarkar, M.Z. Effects of welding technique, filler metal and post-weld heat treatment on stainless steel and mild steel dissimilar welding joint. *J. Manuf. Process.* **2021**, *64*, 1307–1321. [CrossRef]
6. Liu, G.W.; Li, W.; Qiao, G.J.; Wang, H.J.; Yang, J.F.; Lu, T.J. Microstructures and interfacial behavior of zirconia/stainless steel joint prepared by pressureless active brazing. *J. Alloy. Compd.* **2009**, *470*, 163–167. [CrossRef]
7. Liu, D.; Long, W.; Wu, M.; Qi, K.; Pu, J. Microstructure Evolution and Lifetime Extension Mechanism of Sn-Added Fe-Based Pre-Alloy Brazing Coating in Diamond Tools. *Coatings* **2019**, *9*, 364. [CrossRef]
8. Long, W.M.; Zhang, G.X.; Zhang, Q.K. In situ synthesis of high strength ag brazing filler metals during induction brazing process. *Scr. Mater.* **2015**, *110*, 41–43. [CrossRef]
9. Huang, Y.; Liang, G.; Lv, M.; Al-Nehari, M.; Xiao, C. Comparative study on the joining performance of TiH_2 and ZrH_2 modified AgCu28 brazing alloys with pulsed laser welding-brazing. *J. Manuf. Process.* **2019**, *41*, 56–65. [CrossRef]
10. Lin, J.; Ba, J.; Cai, Y.; Ma, Q.; Luo, D.; Wang, Z.; Qi, J.; Cao, J.; Feng, J. Brazing SiO_{2f} /SiO_2 with TC4 alloy with the help of coating graphene. *Vacuum* **2017**, *145*, 241–244. [CrossRef]
11. Lin, P.; Lin, T.; He, P.; Wang, M.; Yang, J. Microstructure evolution and mechanical properties of a vacuum-brazed Al_2O_3/Ti joint with Mo-coating on Al_2O_3 and Ti surfaces. *Ceram. Int.* **2019**, *45*, 11195–11203. [CrossRef]
12. Zhao, L.; Zhang, L.; Tian, X.; Peng, H.; Feng, J. Interfacial microstructure and mechanical properties of joining electroless nickel plated quartz fibers reinforced silica composite to invar. *Mater. Des.* **2011**, *32*, 382–387. [CrossRef]
13. Cheng, F.; Sun, J. Fabrication of a double-layered Co-Mn-O spinel coating on stainless steel via the double glow plasma alloying process and preoxidation treatment as SOFC interconnect. *Int. J. Hydrogen Energy* **2019**, *44*, 18415–18424. [CrossRef]
14. Sun, Z.; Cao, Y.; Zhang, L.; Feng, J. Carbothermal reduction reaction enhanced wettability and brazing strength of AgCuTi-SiO_{2f}/SiO_2. *J. Eur. Ceram. Soc.* **2020**, *40*, 1488–1495. [CrossRef]
15. Xin, C.; Li, N.; Jia, J.; Du, J.; Yan, J. Interfacial microstructures formation mechanism between SiO_2 substrate and AgCuTi braze alloys. *Ceram. Int.* **2018**, *44*, 17784–17791. [CrossRef]
16. Lee, J.G.; Lee, M.K. Microstructure and mechanical behavior of a Titanium-to-stainless steel dissimilar joint brazed with Ag-Cu alloy filler and an Ag interlayer. *Mater. Charact.* **2017**, *129*, 98–103. [CrossRef]

17. Yuan, X.; Kang, C.Y.; Kim, M.B. Microstructure and XRD analysis of brazing joint for duplex stainless steel using a Ni–Si–B filler metal. *Mater. Charact.* **2009**, *60*, 923–931. [CrossRef]
18. Yang, J.; Xu, Y.; Zhang, S.; Zhang, M. Brazing of Mn–Cu alloy and 430 stainless steel with Cu–34Mn–6Ni–10Sn filler metal. *Mater. Trans.* **2019**, *60*, 1674–1679. [CrossRef]
19. Yang, J.; Xu, Y.; Zhang, S.; Zhang, M. Joining of Mn-Cu alloy and 430 stainless steel using Cu-based filler by SIMA-imitated brazing process. *Mater. Lett.* **2019**, *253*, 401–404. [CrossRef]
20. Shi, H.; Yan, J.; Ning, L.; Xin, Z.; Chen, K.; Yu, L. Microstructure and properties of FeCrMo damping alloy brazing joint using Mn-based brazing filler. *Vacuum* **2019**, *159*, 209–217. [CrossRef]
21. Lin, C.; Shiue, R.K.; Wu, S.K.; Lin, Y.S. Dissimilar infrared brazing of CoCrFe(Mn)Ni equiatomic high entropy alloys and 316 stainless steel. *Crystals* **2019**, *9*, 518. [CrossRef]
22. Li, Y.; Parfitt, D.; Flewitt, P.E.J.; Hou, X.; Fonseca, J.Q.D.; Chen, B. Microstructural considerations of enhanced tensile strength and mechanical constraint in a copper/stainless steel brazed joint. *Mater. Sci. Eng. A Struct.* **2020**, *796*, 139992. [CrossRef]
23. Jameson, G.J.; Cerro, M. Theory for the equilibrium contact angle between a gas, a liquid and a solid. *J. Chem. Soc. Faraday Trans.* **1976**, *1*, 883–895. [CrossRef]
24. Gao, Y.; Liang, Y.; Shi, C. Microstructure of laser remelted Ni-base alloy coating on stainless steel. *J. Mater. Sci. Technol.* **1998**, *1*, 49–52. [CrossRef]
25. Si, X.Q.; Cao, J.; Kiebach, R.; Xu, Y.; Xu, H.; Talic, B.; Feng, J. Joining of solid oxide fuel/electrolysis cells at low temperature: A novel method to obtain high strength seals already at 300 °C. *J. Power Sources* **2018**, *400*, 296–304. [CrossRef]
26. Molleda, F.; Mora, J.; Molleda, J.R.; Carrillo, E.; Mora, E.; Mellor, B.G. Copper coating of carbon steel by a furnace brazing process using brass as the braze. *Mater. Charact.* **2008**, *59*, 613–617. [CrossRef]
27. Li, J.; Pan, L.; Fu, Q.; Zhou, Y.; Guo, N. Wettability and corrosion behavior of a Ni coating on 304 stainless steel surface. *Surf. Coat. Technol.* **2018**, *357*, 740–747. [CrossRef]
28. Yu, G.; Zou, T.; Chen, S.; Huang, J.; Zhao, Z. Effect mechanism of Ni coating layer on the characteristics of Al/steel dissimilar metal brazing. *Mater. Charact.* **2020**, *167*, 110518. [CrossRef]
29. Zhao, X.; Tan, C.; Xiao, L.; Xia, H.; Bo, C.; Song, X.; Li, L.; Feng, J. Effect of the Ni coating thickness on laser welding-brazing of Mg/steel. *J. Alloy. Compd.* **2018**, *769*, 1042–1058. [CrossRef]
30. Kim, C.; Suh, B.L.; Yun, H.; Kim, J.; Lee, H. Surface plasmon aided ethanol dehydrogenation using Ag-Ni binary nanoparticles. *ACS Catal.* **2017**, *7*, 2294–2302. [CrossRef]
31. Bracq, G.; Laurent-Brocq, M.; Perrière, L.; Pirès, R.; Joubert, J.M.; Guillot, I. The FCC solid solution stability in the Co-Cr-Fe-Mn-Ni multi-component system. *Acta Mater.* **2018**, *128*, 327–336. [CrossRef]
32. Wu, T.; Zhang, X.; Yuan, Q.; Xue, J.; Lu, G.; Liu, Z.; Wang, H.; Ding, F.; Yu, Q. Fast growth of inch-sized single-crystalline graphene from a controlled single nucleus on Cu-Ni alloys. *Nat. Mater.* **2015**, *15*, 43–48. [CrossRef] [PubMed]
33. Venkateswaran, T.; Vincent, X.; Sivakumar, D.; Bhanu, P.; Janaki, G.D.R. Brazing of stainless steels using Cu-Ag-Mn-Zn braze filler: Studies on wettability, mechanical properties, and microstructural aspects. *Mater. Des.* **2017**, *121*, 213–228. [CrossRef]
34. Wenzel, R.N. Resistance of solid surfaces to wetting by water. *Ind. Eng. Chem.* **1936**, *28*, 988–994. [CrossRef]
35. Cassie, A.B.D.; Baxter, S. Wettability of porous surfaces. *Trans. Faraday Soc.* **1944**, *40*, 546–551. [CrossRef]
36. Khodaei, M.; Shadmani, S. Superhydrophobicity on aluminum through reactive etching and TEOS/GPTMS/nano-Al_2O_3 silane-based nanocomposite coating. *Surf. Coat. Technol.* **2019**, *374*, 1078–1090. [CrossRef]
37. Liu, Y.; Bai, Y.; Jin, J.; Tian, L.; Han, Z.; Ren, L. Facile fabrication of biomimetic superhydrophobic surface with anti-frosting on stainless steel substrate. *Appl. Surf. Sci.* **2015**, *355*, 1238–1244. [CrossRef]
38. Mirski, Z.; Piwowarczyk, T. Wettability of hardmetal surfaces prepared for brazing with various methods. *Arch. Civ. Mech. Eng.* **2011**, *11*, 411–419. [CrossRef]
39. Ma, Q.; Tong, Z.; Wang, W.; Dong, G. Fabricating robust and repairable superhydrophobic surface on carbon steel by nanosecond laser texturing for corrosion protection. *Appl. Surf. Sci.* **2018**, *455*, 748–757. [CrossRef]
40. Wang, H.; Zhuang, J.; Qi, H.; Yu, J.; Ma, Y. Laser-chemical treated superhydrophobic surface as a barrier to marine atmospheric corrosion. *Surf. Coat. Technol.* **2020**, *401*, 126255. [CrossRef]
41. Wang, C.X.; Zhang, X.F. A non-particle and fluorine-free superhydrophobic surface based on one-step electrodeposition of dodecyltrimethoxysilane on mild steel for corrosion protection. *Corros. Sci.* **2020**, *163*, 108284. [CrossRef]
42. Wang, H.; Zhu, Y.; Hu, Z.; Zhang, X.; Wu, S.; Wang, R.; Zhu, Y. A novel electrodeposition route for fabrication of the superhydrophobic surface with unique self-cleaning, mechanical abrasion and corrosion resistance properties. *Chem. Eng. J.* **2016**, *303*, 37–47. [CrossRef]
43. Sun, Y.; Liu, J.; Ming, P.; Zhao, D.; Song, J. Wire electrochemical etching of superhydrophobic 304 stainless steel surfaces based on high local current density with neutral electrolyte. *Appl. Surf. Sci.* **2022**, *571*, 151269. [CrossRef]
44. Li, H.; Xu, W.; Li, L.; Xia, H.; Chen, X.; Chen, B.; Song, X.; Tan, C. Enhancing the wettability for 4043 aluminum alloy on 301L stainless steel via chemical-etched surface texturing. *J. Mater. Process. Technol.* **2022**, *305*, 117577. [CrossRef]
45. Liu, Z.; Yang, J.; Li, Y.; Li, W.; Chen, J.; Shen, L.; Zhang, P.; Yu, Z. Wetting and spreading behaviors of Al-Si alloy on surface textured stainless steel by ultrafast laser. *Appl. Surf. Sci.* **2020**, *520*, 146316. [CrossRef]
46. Roy, R.K.; Panda, A.K.; Govind, S.K.D.; Mitra, A. Development of a copper-based filler alloy for brazing stainless steels. *Mater. Sci. Eng. A Struct.* **2009**, *523*, 312–315. [CrossRef]

47. Zheng, Y.; Li, N.; Yan, J.; Cao, Y. The microstructure and mechanical properties of 1Cr17Ni2/QAl7 brazed joints using Cu-Mn-Ni-Ag brazing alloy. *Mater. Sci. Eng. A Struct.* **2016**, *661*, 25–31. [CrossRef]
48. Miao, W.; Zheng, S.; Zhou, J.; Zhang, B.; Fang, R.; Hao, D.; Sun, L.; Wang, D.; Zhou, Z.; Xu, J.; et al. Microchannel and nanofiber array morphology enhanced rapid superspreading on animals' corneas. *Adv. Mater.* **2021**, *33*, 2007152. [CrossRef]